Determinants of Combination GM-CSF Immunotherapy and Oncolytic Virotherapy Success Identified Through *In Silico* Treatment Personalization

Tyler Cassidy[1] and Morgan Craig[2,3]

[1]Department of Mathematics and Statistics, McGill University, Montréal, Canada,
[2]Département de mathématiques et de statistique, Université de Montréal, Canada
[3]Department of Physiology, McGill University, Canada

Running title: Determinants of Combination Immunotherapy Success Identified Through *In Silico* Personalization
Morgan Craig: Département de mathématiques et de statistique, Université de Montréal, Pavillon André-Aisenstadt, Case postale 6128, succursale Centre-ville Montréal Canada, 1-514-343-7471, morgan.craig@umontreal.ca
Word count: 4328, 6 Figures, 2 Tables

Abstract

Oncolytic virotherapies, including the modified herpes simplex virus talimogene laherparepvec (T-VEC), have shown great promise as potent instigators of anti-tumour immune effects. The OPTiM trial demonstrated the superior anti-cancer effects of T-VEC as compared to more traditional immunotherapy treatment using exogenous administration of granulocyte-macrophage colony-stimulating factor (GM-CSF). Theoretically, a combined approach leveraging exogenous cytokine immunotherapy and oncolytic virotherapy would elicit an even greater immune response and improve patient outcomes. However, given that regimens of combination GM-CSF and T-VEC therapy must be evaluated in large clinical trials to evaluate efficacy and safety, therapeutic regimens have yet to be established. Here, we calibrate a computational biology model of sensitive and resistance tumour cells and immune interactions that is implemented into an *in silico* clinical trial approach. By personalizing and optimizing combination oncolytic virotherapy and GM-CSF therapy, we show improved simulated patient outcomes for individuals with late-stage melanoma. More crucially, through evaluation of individualized regimens, we identified determinants of combination GM-CSF and T-VEC therapy that can be translated into clinically-actionable dosing strategies without further personalization. Our results serve as a proof-of-concept for interdisciplinary approaches to determining combination therapy, and suggest promising avenues of investigation towards tailored combination immunotherapy/oncolytic virotherapy. *Keywords*: *in silico* trial, computational biology, combination therapy, treatment scheduling

Introduction

To cite: Dingli2009b, Venkatasubramanian2010, Basanta2012 These aren't cited, can you please add in references?

Modern cancer treatments increasingly incorporate a broad class of biological therapies known as immunotherapies to activate the immune system against cancer cells in a generalized or targeted way.[3,4] These therapies seek to exploit existing tumour-immune interactions to more effectively recognize and destroy tumour cells with the goal of minimizing off-target and detrimental side effects. Current and investigational immunotherapies include immune-checkpoint inhibitors, monoclonal antibodies, CAR-T cells, and the exogenous administration of cytokines. One such cytokine, granulocyte-macrophage colony-stimulating factor (GM-CSF), is a white blood cell growth factor responsible for stimulating granulocyte production, and orchestrating innate inflammatory responses. GM-CSF has been used to increase the efficacy of monoclonal antibodies, and has also been administered during B-cell lymphoma treatment to activate certain immune cell subsets.[4]

Another older idea, recently adopted in clinical applications, is to use oncolytic viruses to destroy tumour cells[5,6] and activate an immune response. These oncolytic viruses are genetically engineered to preferentially attack and infect cancerous cells,[7,8] forcing infected cells to undergo lysis and release tumour specific antigens that signal the immune system to mount an anti-tumour response.[9,10] This double effect against tumour cells has propelled the study of oncolytic viruses as a treatment against a variety of malignant solid tumours.

Subsequently, the modified herpes simplex virus talimogene laherparepvec (T-VEC) was approved for use in patients with non-resectable melanoma in 2015.[11–13] T-VEC is specifically engineered to enhance expression of GM-CSF after viral infection into tumour cells.[11] However, despite much promise, the efficacy of oncolytic virus monotherapy has been limited.[10,14,15] As it is reasonable to expect that immunotherapy and virotherapy could act synergistically to instigate an immune response against tumour cells,[16–18] recent efforts have focused on determining the anticipated benefit to their use in combination with a variety of immunotherapies.[19,20] To that end, GM-CSF has been considered as an immune stimulant during oncolytic virotherapy.[4]

Generally speaking, combination therapy can carry a high therapy burden and may increase overall toxicity.[15,20] Unfortunately, running clinical trials for all possible (dose,time)-pairs of a proposed combined treatment to determine efficient and safe scheduling is both time and cost prohibitive. As a consequence, regimen scheduling of combination immuno-/oncolytic virotherapy remains an open problem. There is an established history of applications of modelling-based, scomputational biology approaches to the *in silico* determination of potential therapeutic schedules that concretely improve patient outcomes.[21–24] More recently, by employing a straight-forward evolutionary game theory model to determine adaptive treatment schedules, Zhang et al.[25] report significant improvements to prostate specific antigen in comparison to the standard-of-care in an on-going phase I clinical trial. This and other[?] successes motivate the continued application of interdisciplinary approaches in personalized oncology. Perhaps the most significant impact made by quantitative methodologies is the identification and translation of the underlying determinants of treatment success into actionable therapeutic strategies.[26,27]

To that end, here we detail the rationalization of combination immuno-/virotherapy scheduling for patients with late-stage melanoma by implementing an *in silico* clinical trial. By integrating our previous computational biology model of sensitive and resistance tumour cells and their interactions with the immune system into our virtual trial platform, we generated identical virtual patient cohorts to determine optimal, individualized treatment regimens for combined GM-CSF immunotherapy and T-VEC. We used the results of the personalization to infer a logical and clinically actionable dosing scheme that significantly improved overall survival and progression free survival while substantially reducing drug burden. Crucially, we identified key mechanisms determining therapy success, allowing us to define a successful regimen in a new patient cohorts. Our results highlight the potential and potency of rational regimen prediction using a computational biology approach, and serve as a proof-of-concept for future quantitative studies in oncology.

Materials and Methods

Computational Biology Model

To establish the synergistic interactions elicited between immunotherapy (exogenous GM-CSF) and oncolytic virotherapy, we adapted our previous mathematical model[28] describing

the instantaneous change in tumour size, phagocyte numbers and cytokine concentrations over time. The model tracks both immuno-susceptible and immuno-resistant tumour cell populations as they progress through the cell cycle. Quiescent immuno-susceptible tumour cells can be cleared through either random death or immune pressure, or transit into the G_1 phase to begin reproduction. Cells in G_1 are also subject to random death and immune clearance before beginning the mitotic process. After completing division, susceptible cells return to quiescence. Mitotic cells may mutate at rate μ into an immuno-resistant cell type with a low probability. This immuno-resistant lineage maintains the same cell cycle behaviour of non-resistant tumour cells, but is not subject to any immune interactions, as it evades immune pressure. We do not distinguish between different types of immune cells in the tumour microenvironment, but rather model all phagocytes as a single population. These phagocytes interact with the susceptible tumour cell population and produce a pro-inflammatory cytokine (e.g. interleukin-12, tumour necrosis factor, interferon gamma, GM-CSF etc.) to recruit other phagocytes to the tumour site. Model predictions are obtained by simulation, as previously described[28] (full details are provided in the Supplementary Information). The various interactions described above are schematized in Figure 1.

Generation of *In Silico* Individuals and Patient Cohorts

To calibrate the model of Cassidy and Humphries[28] to available data, we adopted a sequentia fitting procedure to parameterize the mathematical model. Briefly, we used time series data from a number of experimental settings to parameterize the different model compartments. We began by determining the parameters of the delay kernel using data from a cervical cancer cell line **CITATIONS**, before fitting the remaining parameters in a sequential manner. First, data from tumour growth in immuno-compromised mice was used to fit the tumour growth parameters a_1, a_2, and d_2. Next, we fit the viral parameters **WHICH?** using a combination of *in vitro* data from Toda et al. and Randazzo et al.[43,44] Finally, we used data from GM-CSF concentrations following administration of a T-VEC precursor in mice to fit the parameters for the cytokine compartment. In each case, we reduced the mathematical model to replicate the experimental set up, and minimized the least-squares error between simulations and experimental data (for extended details, see the Supplementary Information).

To reflect the interindividual variability and heterogenous nature of patient cohorts, we individualized the model by generating a unique set of parameters to represent single patients. To create individuals in the *in silico* clinical trial, we sampled each of the model's parameters from a generated normal distribution with mean $\hat{\mu}$ determined in the sequential fitting procedure. We then defined $\mathbf{p}$ to be the vector of fitted parameter values[28] and parametrized the normal distributions so that 99.7% of patients fall within $[\mu - 3\sigma, \mu + 3\sigma] = [0.5\mathbf{p}, 1.5\mathbf{p}]$. If empirical information about a parameter's distribution was available, this measurement was used in lieu of the previously described procedure. Each individual is then created by sampling each model parameter from this distribution. We confirmed that using this methodology created virtual patients with parameter values following an approximately normal distribution about the mean empirical or fitted value, as shown in Figure 2. The distribution

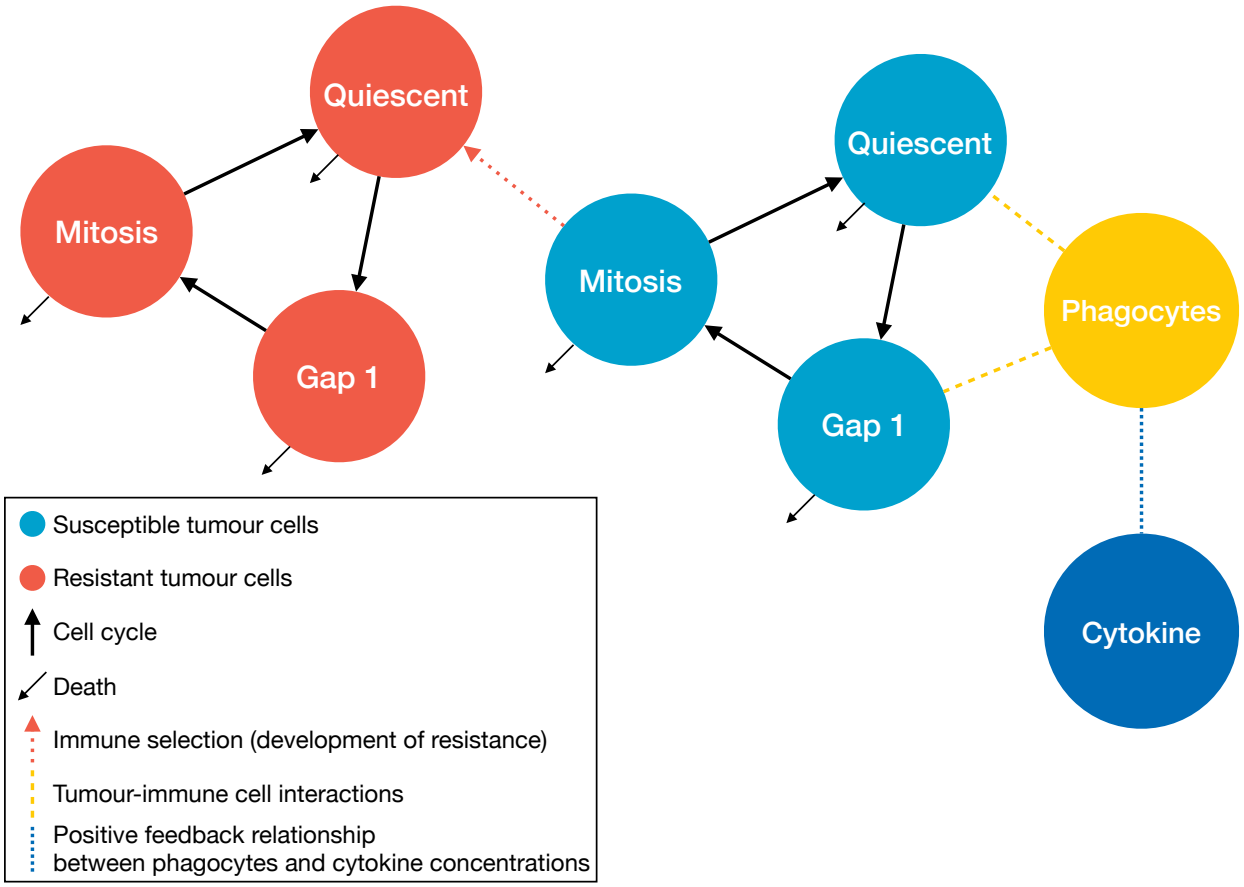

Figure 1: **Pictorial representation of the tumour growth model.** Quiescent cells activate to begin division by transiting into the G_1 phase of the cell-cycle. Cells exit G_1 to enter the active phase and complete division. Most susceptible cells in the active phase re-enter quiescence after mitosis, however certain dividing cells may mutate into an immuno-resistant lineage (red dotted arrow). Immune interactions are driven by phagocytes who come into contact with quiescent and G_1 phase susceptible cells (dashed yellow lines). Tumour-immune interactions increase pro-inflammatory cytokine concentrations to recruit additional phagocytes to the tumour site (blue dotted line). Cells and cytokine are denoted by circles, processes by squares, and rates by arrows.

of parameters approximates the empirical distribution used to define the virtual population, indicating that this virtual patient generation procedure produces a representative sample of the possible virtual population (and not multiples of the same individual).

To further protect against the creation of nonrealistic virtual patients, we imposed selection and inclusion criteria on each generated individual by verifying that each virtual patient responds in a physiologically-realistic way without and with treatment.[21] Specifically, we compared the predicted response of each virtual patient to currently approved oncolytic virotherapy for stage IIIb or IV non-surgically resectable melanoma.[10,11] Moreover, we assessed whether the predicted tumour doubling time of each individual corresponded to clinically relevant tumour doubling times,[29] and used this comparison as the sole inclusion criterion for subsequent enrolment *in silico* clinical trial simulations. To ensure that we were sampling

from the entirety of the physiologically realistic portion of parameter space,[21] we performed a local sensitivity analysis to determine the impact of parameter variation on model output (see the Supplementary Information).

We accepted a total of 300 virtual patients, generated by the parameter sampling and selection processes outlined above. Each virtual patient was then reproduced into n identical clones, and each resulting clone was subsequently assigned to one of n separate cohorts (for example, a treatment free control group, a mono-immunotherapy group, and an oncolytic virotherapy group, for a total of $n = 3$ cohorts). In this way, the total number of participants is 300 times the total number of simulated investigational arms, or $300n$. The *in silico* trial generation process is schematized in Figure 2. As these cohorts are identical, we are able to establish the casual relationship between changes in treatment strategy and increased survival time shown in Figure 3 (b).

Recapitulation of Previous Trial Data

Using three identical cohorts, we evaluated patient outcomes when they received no treatment (Cohort 1), immunotherapy (Cohort 2), or oncolytic virus monotherapy (Cohort 3) to mimic the T-VEC OPTiM trial, where individuals were randomized to receive either intralesional T-VEC or subcutaneous GM-CSF.[11]

In both the *in silico* immunotherapy and oncolytic virus monotherapy cases, the dosing schedules were identical to the ones used in the OPTiM trial:[11] patients in the T-VEC arm received a priming dose of 10^6 plaque forming units pfu/mL, followed by 10^8 pfu/mL doses to a maximal total administration of 4 mL per treatment. T-VEC was administered every 14 days. Patients in the GM-CSF arm received 125 μg/m^2 of subcutaneous GM-CSF administered on 14 consecutive days followed by 14 days of no treatment. In both arms, treatment continued for up to 12 months but could be discontinued due to disease progression, intolerability, or the disappearance of injectable lesions. The median treatment length for the T-VEC and GM-CSF arms were 23 and 10 weeks respectively.

We fixed an oncolytic virotherapy dose of 250×10^6 virions – which corresponds to roughly 1×10^6 pfu[30]– as the amount of virus administered the original trial varied based on both patients and physicians.[11] Note that the units between the OPTiM trial[11] and our *in silico* trial differ owing only to the units of the mathematical model's parameters and the conversion of pfu to infectious virions. Individuals receiving GM-CSF immunotherapy in the *in silico* trial were administered 125 μg/m^2 of GM-CSF daily for 14 days in 28 day cycles. For both arms, we simulated the model over a fixed treatment time of 6 months.

Late stage melanoma has a low survival rate.[31] Mortality as a function of tumour doublings has been estimated to occur between 40 and 45 tumour doublings.[29,32,33] Given that roughly 30 doublings occur before clinical presentation,[33] we estimated that there are approximately 10 and 15 tumour doublings between diagnosis and death. *In silico* patients were therefore removed from the simulated trial after their predicted tumour size reached 2^λ, where λ denotes the removal number of tumour doublings for each individual. For each individual, this fatal number λ was obtained by sampling uniformly from $\{10, 11, 12, 13, 14, 15\}$, or the

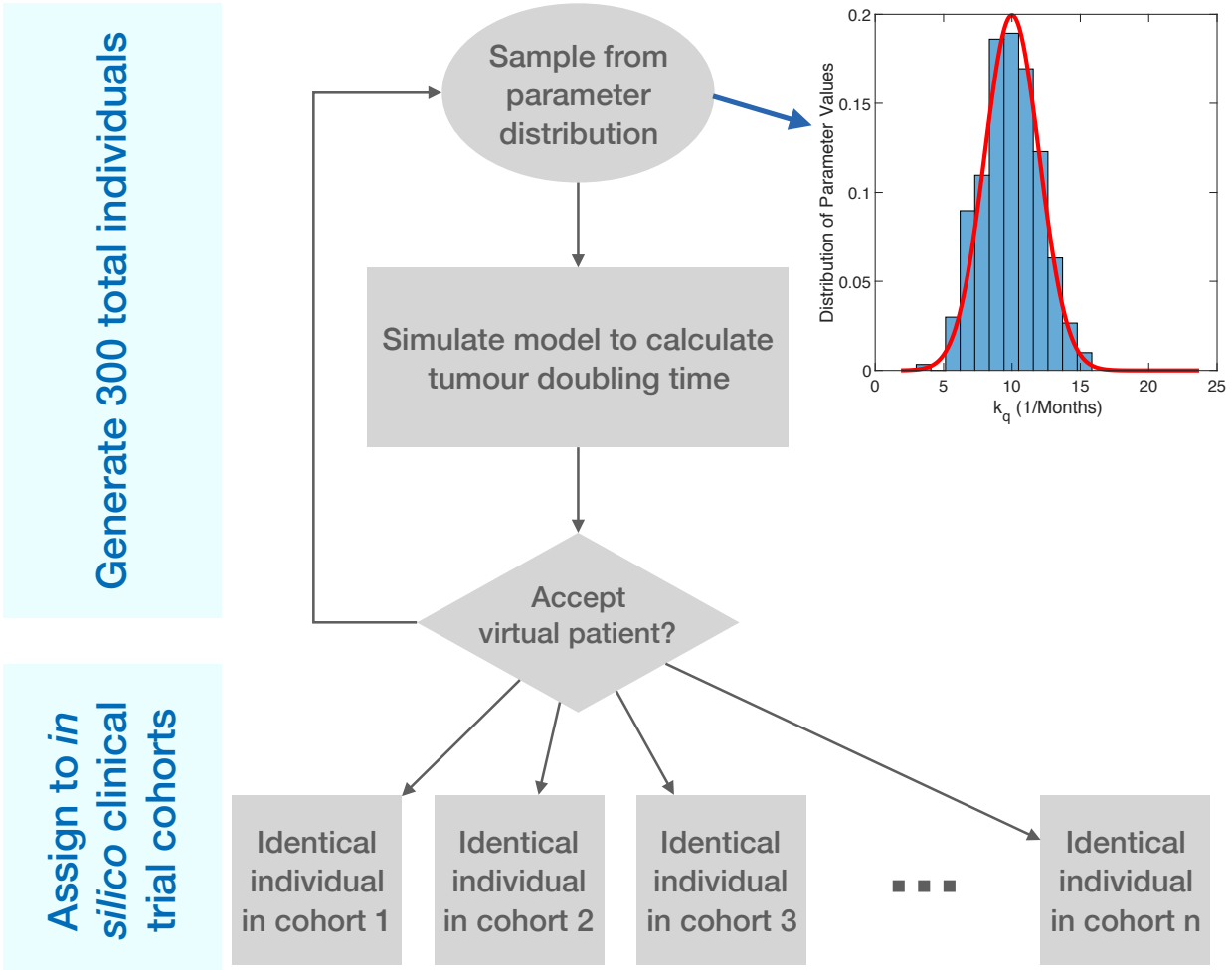

Figure 2: **A pictoral representation of the *in silico* patient creation algorithm.** Individual *in silico* patient parameter values are sampled from a normal distribution of values based on an average parameterization.[28] The model was then simulated for each individual and tumour growth predictions (tumour doubling time) were tested for physiological relevance. If the *in silico* patient's tumour growth behaviour was considered physiologically realistic, they were cloned n times and each clone was assigned to n separate arms of the *in silico* clinical trial.

set of possible tumour doubling values between diagnosis and death. **What happened to the RECIST criteria?** The incorporation of different disease stages in the OPTiM trial is discussed in the Supplementary Information.

Optimization Routine for Combined Immuno- and Oncolytic Virotherapies

Adverse effects reported in the OPTiM trial including fatigue, chills and other flu like symptoms. Grade 3 adverse effects occurred in 36% and 21% of patients receiving T-VEC and GM-CSF respectively. To provide maximal therapeutic benefit with the lowest possible treat-

ment burden, we defined individualized dosing regimens to be the schedule that minimizes the cumulative tumour burden (the area under the total tumour curve) and the cumulative dose (the total amount of therapy administered over the treatment time). The minimized function was given by

$$F(\text{Dose}) = \text{Cumulative Tumour Burden} + \alpha\text{Cumulative Dose},$$

where the positive scaling coefficient α weights the importance of maximizing the therapeutic effect versus the need to minimize treatment burden. These weighting values take into account the need for a treatment to be simultaneously effective and tolerable.

Tolerability of combined therapy was attained by bounding the permissible dose size to be four times the standard dose amount, consistent with the maximum dose for T-VEC in the OPTiM trial. As it is only possible to administer discrete amounts of a drug, typically limited to be some multiple of the available vial size, we constrained the dose size to be $1-4$-times the standard dose size for both immunotherapy and virotherapy. We allowed for daily immunotherapy dosing and restricted virotherapy administration to days 7, 14, 21, 28, 35, 42, 49, 56, 63, 70 so that virotherapy defined the beginning of a week-long treatment cycle. In total, there are 2000 possible treatment cycles, given that 200 virtual patients underwent ten treatment cycles. Note that the schedule described above is potentially denser than what was administered by Andtbacka et al.[11] To study whether denser treatment scheduling improved clinical outcomes, we allowed for increased treatment frequency, under the constraint that the cumulative dose administered in the optimal treatment regimen must be less than the cumulative dose administered during the OPTiM trial.[11]

Genetic algorithms are heuristic global optimization routines inspired by natural selection[34–36] that are frequently employed to estimate parameters in computational biology models. They have also previously been applied to study optimal dosing routines in immunology.[36] To determine personalized dosing regimens, the optimal function $F(\text{Dose})$ was minimized over a ten-week treatment period using Matlab's genetic algorithm function *ga*.[37]

We then generated personalized schedules for each of the 300 individuals in the optimal combination cohort. These schedules determined an underlying statistical distribution of the likelihood of administering a dose of either immuno- or virotherapy on a given day of the treatment period. Sampling from this empirical distribution, we next determined the probability that immunotherapy, $P_I(\text{Day}_i)$, or virotherapy, $P_V(\text{Day}_i)$, is administered on Day i of therapy to determine a probabilistic treatment schedule that replicated the results of the treatment optimization on the population-level.

Inference and Validation of Optimal Treatment Schedule

We first determined whether a dose of immunotherapy was to be administered on the i-th day of treatment by sampling from a Bernoulli distribution with probability given by $P_I(\text{Day}_i)$ (see Table 1). If a dose was administered, we sampled from the empirical distribution of dose sizes determined from the individualization (see previous section) with weights $P_I(n|\text{Day}_i)$ (i.e. the probability of giving a dose of size n given that immunotherapy is administered on day i) to determine the size of the immunotherapy size. If the i-th day is the beginning

of a new treatment cycle, virotherapy may be administered. If so, the same series of steps determined whether virotherapy was administered, and if so, the size of dose, based on $P_V(\text{Day}_i)$.

To test the effectiveness of the probabilistic dosing schedule, we created and cloned 200 new virtual patients, and separated them into three three trial arms. The first cohort received the combined immuno- and virotherapy of 125 μg/m^2 of GM-CSF daily for 14 days in 28 day cycles and 1 dose of virotherapy every 14 days corresponding to a combination of the standard of care reported in the OPTiM trial.[11] A maintenance therapy schedule was derived from the results of the therapy optimization and was followed for the second cohort (see *Results*). Finally, the probabilistic dosing regimen determined from the population optimization was applied to the third arm. In the all three arms, virtual patients received treatment for the median treatment duration of the OPTiM trial. Mortality and removal from the trial followed the same procedure described in the *Model Calibration* section above.

Results

Computational Biology Model Successfully Predicts Existing Therapy Results

We first compared the model predictions to the OPTiM results[11] to evaluate the computational biology model's ability to accurately represent the outcomes for patients receiving either GM-CSF or the oncolytic virus monotherapy T-VEC.[11,13] Fig. 3A summarizes the predicted survival curves of both treatment arms. Unsurprisingly, no untreated virtual patient survived to the end of the trial (not shown) and both of the treated cohorts display increased survival when compared to no treatment. Patients receiving virotherapy were the most likely to survive until the end of the *in silico* trial. The median survival time for patients in the T-VEC cohort of the *in silico* trial was 39.0 months, as compared to the reported median overall survival time of 41.1 months for patients with stage IIIB, IIIC, or IVM1a melanoma in the OPTiM trial. The median survival time for patients in the GM-CSF arm of the *in silico* clinical trial was 31.3 months, just outside of the 95% confidence interval of 17.4 to 29.6 months of the OPTiM trial. The null hypothesis that T-VEC and GM-CSF have the same efficacy was rejected with $p < 0.001$ using a log-rank test.

To measure the time from treatment initiation to failure, we considered the time from beginning of treatment until the tumour contains twice the initial number of tumour cells. The median time to treatment failure was then predicted to be 2.9 (OPTiM trial: 8.2 with 95% confidence interval of 6.5-9.9) and 13.9 months (OPTiM trial: 2.9 with 95% confidence interval of 2.8-4.0) in the GM-CSF and T-VEC arms, respectively.

The relative treatment benefit for survival time under virotherapy against the survival time under immnuotherapy for each virtual patient is presented in Fig. 3B. Virtual patients were ordered according to their untreated tumour doubling time, where a longer doubling time indicated slower progression and less aggressive disease. A line of best fit indicates that oncolytic virus therapy provided larger survival gains in those with with longer doubling

times when compared to GM-CSF, which is consistent with the increased survival fraction of patients with stage 3 melanoma in Figure 4(f) of Andtbacka et al.[11]

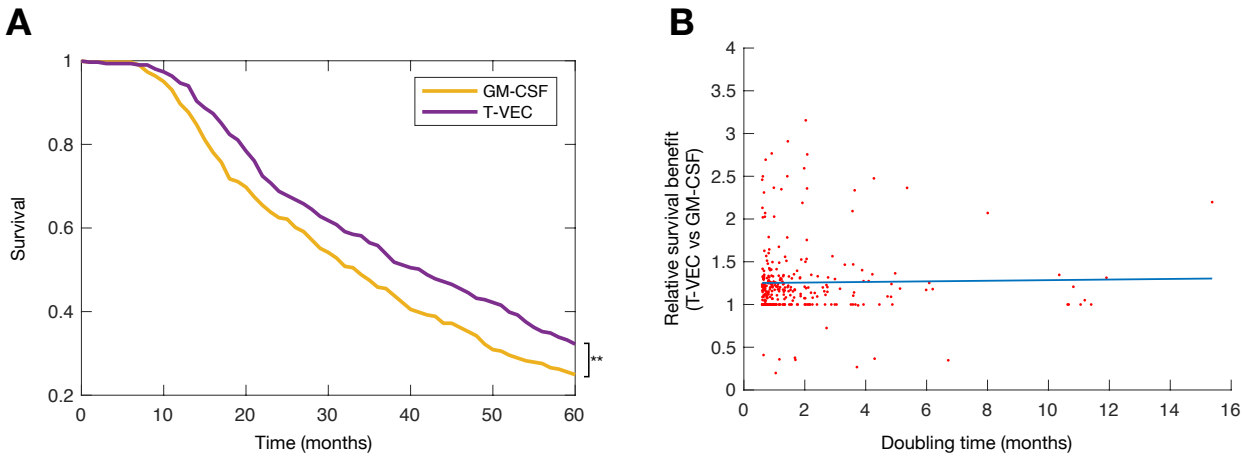

Figure 3: **Treatment with oncolytic virus provides improves outcomes over no treatment and immunotherapy in virtual clinical trial. A)** Kaplan-Meier curves for patients in the no treatment, immunotherapy and virotherapy arms of the virtual trial; **B)** The relative survival benefit for identical virtual patients. We plot the ratio of survival time on T-VEC against survival time on GM-CSF for identical virtual patients and establish a casual relationship between treatment type and survival time. A line of best fit with slope 0.0035 indicates that oncolytic virus therapy provided larger survival gains in those with with longer doubling times when compared to GM-CSF.

"All or Nothing" Virotherapy Dosing Strategy

We expected that treatment with GM-CSF would be used to either prime the immune system before virotherapy, or to support the immune response directly following administration of the oncolytic virus. However, as seen in Fig. 4 and Tab. 1, no structure is easily discerned. To better understand the underlying distribution structure of the individualized treatment schedules, we calculated the probability that any immunotherapy should be administered on each of the seven treatment cycle days of the optimized therapy regimen, as described in the Methods section (*Optimization Routine for Combined Immuno- and Oncolytic Virotherapy*). If a dose was given, we computed the conditional probability of administering a dose of one, two, three or four multiples of the standard dose and report these probabilities in Table 1. We found that the probability of administering a dose of immunotherapy for a given treatment day is roughly constant at 19% throughout the treatment cycle. Interestingly, our results indicate that the immunotherapy dose given is expected to be either the smallest or the largest permitted (see Tab. 1), suggesting that immunotherapy is most useful as an additional instigator when virotherapy does not elicit a sufficient immune response, or to otherwise maintain the immune recruitment initiated by successful viral infection and lysis.

Contrary to the mono-immunotherapy dosing schedule, the conditional probabilities $P_V(\text{Day}_i)$ for viral dose size reported in Table 2 are heavily skewed to the maximal tolerable dose. Given

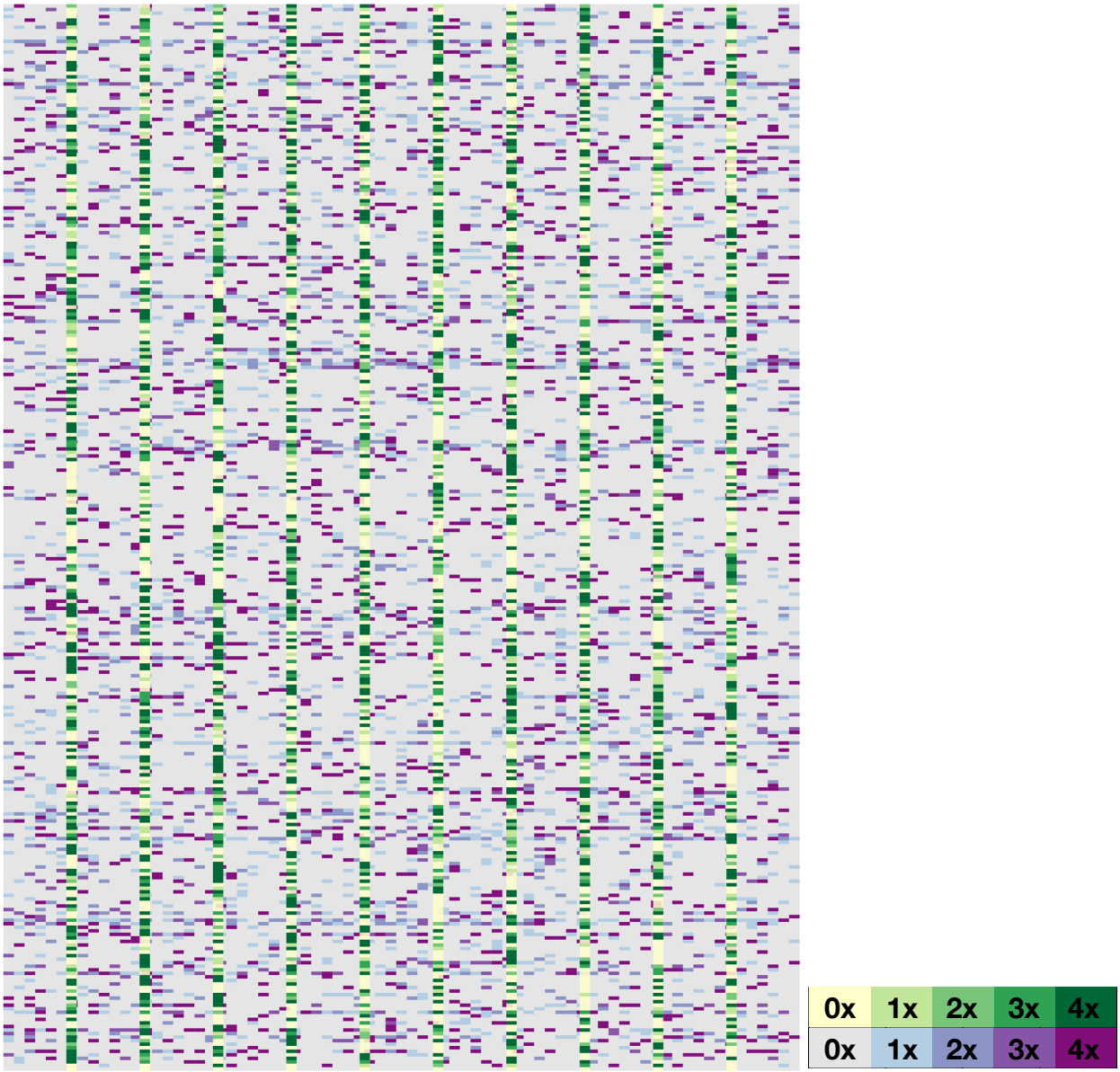

Figure 4: **Optimal personalized dose scheduling for each of the 300 virtual patients.** The nth horizontal row corresponds to the nth virtual patient, while the m-th vertical column corresponds to the dose administered on day m. The dose size is presented as a multiple of the standard dose with immunotherapy in shades of purple and virotherapy in shades of green.

the mechanism of action of virotherapy (namely, infecting tumour cells), it is unsurprising that administering a larger dose of oncolytic virus should improve clinical outcomes. Put differently, an "all or nothing" approach of dosing infrequently, but for maximal therapeutic benefit, is optimal, in contrast to the logic of the immunotherapy case.

These results suggest that administering immunotherapy between administrations of virotherapy serves mainly to maintain immune recruitment.[38] To test this hypothesis, we defined Maintenance Therapy to be the administration of virotherapy once every 14 days

Day_i	-3	-2	-1	Start of Cycle	1	2	3
$P_I(\text{Day}_i)$	0.2043	0.2020	0.2037	0.2027	0.2200	0.2047	0.2057
$P_I(1\|\text{Day}_i)$	0.3719	0.3762	0.3519	0.3799	0.3803	0.3583	0.3387
$P_I(2\|\text{Day}_i)$	0.1599	0.1419	0.1702	0.1694	0.1439	0.1482	0.1929
$P_I(3\|\text{Day}_i)$	0.1550	0.1733	0.1637	0.1217	0.1348	0.1678	0.1378
$P_I(4\|\text{Day}_i)$	0.3132	0.3086	0.3142	0.3289	0.3409	0.3257	0.3306

Table 1: The probability of administering immunotherapy ($P_I(A)$) in each day of the treatment cycle and the conditional probability ($P_I(n|A)$ of administering n doses of immunotherapy for $n = 1, 2, 3, 4$.

with immunotherapy administered evenly throughout on days $3, 6, 9$, and 12 of each virotherapy treatment cycle. Dose size was calculated based on the cumulative expected weekly dose of immunotherapy (8 doses/14 days) from the optimized regimen. Two doses of immunotherapy were therefore administered on days $3, 6, 9$, and 12 to replicate the total expected immunotherapy dose. The same procedure was used to determine the virotherapy dose.

$\mathbf{P_V(\text{Day}_7)}$	**0.5487**
$P_V(1\|\text{Day}_7)$	0.1592
$P_V(2\|\text{Day}_7)$	0.1200
$P_V(3\|\text{Day}_7)$	0.1597
$P_V(4\|\text{Day}_7)$	0.5611

Table 2: **Conditional probabilities for oncolytic virotherapy administration inferred from individualized dose schedule optimization.** The probability of administering virotherapy on each 7th day of the treatment cycle ($P_V(\text{Day}_7)$) and the conditional probability $P_V(n|\text{Day}_7)$ of administering n doses of virotherapy for $n = 1, 2, 3, 4$.

Maintenance and Predictive Combination Therapies Improve Virtual Patient Survival

Despite the shorter treatment period, both the maintenance and probabilistic combination immuno- and oncolytic virotherapies improved overall survival times as compared to the simulated OPTiM trial (see Fig. 3). Maintenance therapy similarly significantly increased mean survival time against mono-virotherapy (47.5 months vs. 35.36 months, two-sided t-test p-value of 1.02×10^{-6}). The maintenance therapy and optimal dosing regimens also outperformed the standard combination therapy: on average, the mean survival time for patients receiving standard combination therapy was 26.1 months, while patients receiving the maintenance therapy or probabilistic dosing survived for 47.5 or 46.6 months respectively (two-sided t-test p-values of $p < 0.001$ in both cases). Survival results for the standard and predicted combination therapies results are summarized in Fig. 5. The hypothesis that the two treatments were equally efficacious was rejected with $p < 0.001$ using a logrank test.

To improve therapy tolerability, an additional criterion for regimen optimality is the minimization of the number of treatment days. In the standard of care schedule, patients received 2 administrations of virotherapy and 14 doses of immunotherapy per 28 day cycle, thus requiring 15 total days of drug administration per 28 day cycle. The maintenance therapy schedule required a total of 11 treatment days per 28 day cycle (9 administrations of immunotherapy and 2 administrations of virotherapy), whereas patients given the optimized treatment schedule were administered an expected 5 immunotherapy doses and 2 virotherapy doses per 28 day cycle, for a total of 9 expected treatment days.

Mean survival times between patients receiving the maintenance therapy and the probabilistic therapy were not significantly different (47.9 months vs 46.7 months, two-sided t-test p-value of 0.754). This is not unsurprising, given that the maintenance therapy was defined directly from the personalized regimens using the "naïve" constraint that immunotherapy be equally spread out throughout each virotherapy cycle. Crucially, the results of the individualized therapy can be translated into a clinically actionable therapeutic strategy that significantly improves simulated clinical outcomes (Maintenance Schedule). While, for a given patient, it may be unsurprising that an optimized and individualized dose predict improved outcomes, leveraging the insights gained from the individualized cohort to produce population-wide improvements on a new cohort is a compelling achievement of our approach.

In summary, in terms of both end-points and dosing burden, immune maintenance therapy outperforms the standard-of-care combination therapy. The equivalency in mean survival times between the maintenance and probabilistic schedules also further motivates the rationalization of therapy scheduling via *in silico* clinical trials to better ascertain the key mechanisms regulating to treatment success prior to clinical trial enrolment.

Discussion

Improving patient end-points and decreasing the drug burden during anti-cancer treatment are crucial components of cancer care. The introduction of new and advanced therapy modalities is critical to this goal. The approval of T-VEC, the first genetically modified oncolytic virus, was an important step forward for the treatment of late-stage melanoma that significantly improved patient survival over mono-immunotherapy GM-CSF administration. However, the question of whether combined immunotherapy and virotherapy will provide further benefits for patients and, if so, the optimal strategy for such combination therapy, remains. Running clinical trials is an expensive and onerous process. Trial failures are disappointing for patients, clinicians, and researchers, and contribute to overall attrition along the drug development pipeline. Here we have outlined a rational approach to therapy optimization that has significant consequences for how we effectively design and implement clinical trials to maximize their success, and how we treat melanoma with combined immuno- and virotherapy.

Leveraging our previous computational biology model, we developed an *in silico* clinical trial by creating virtual individuals based on a realistic distribution of model parameter values. Each generated individual was cloned and assigned to different trial cohorts. This innova-

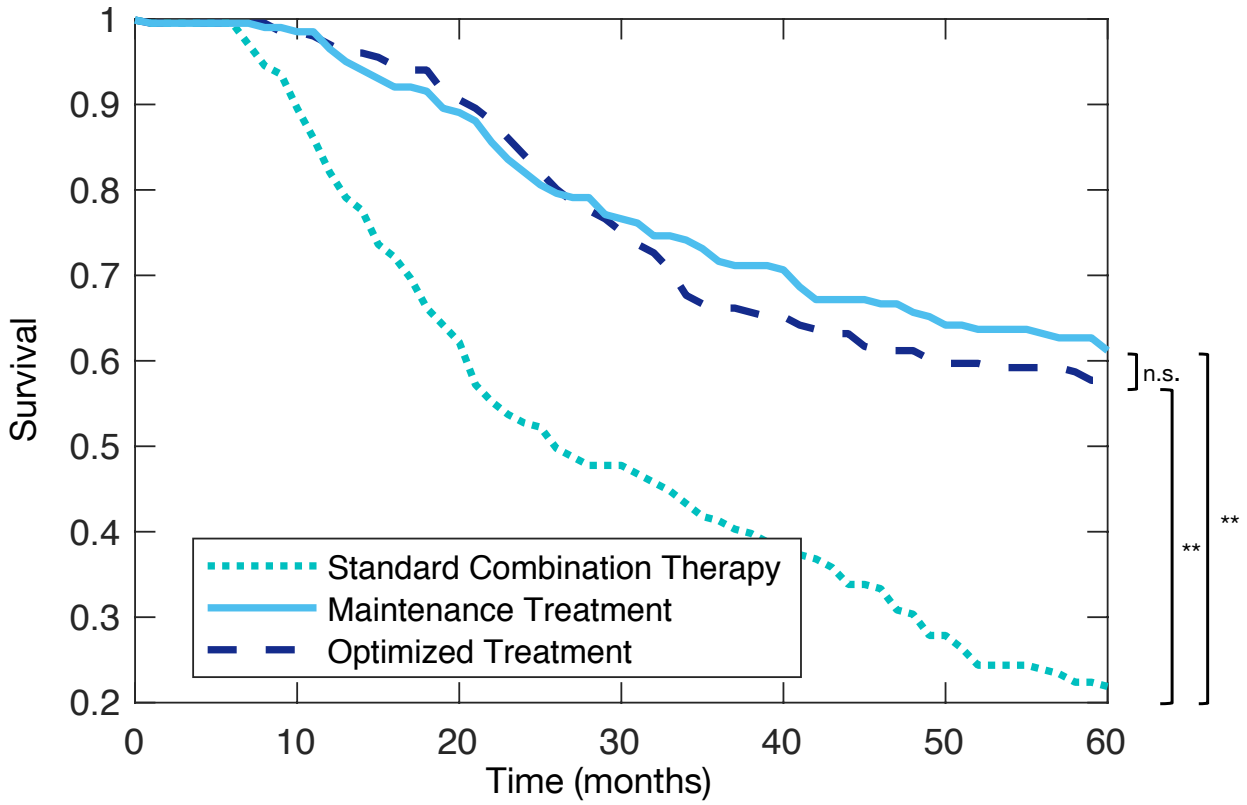

Figure 5: ***In silico* clinical trial predicts improved outcomes for both probabilistic dosing strategies and maintenance therapy versus standard combination therapy.** Kaplan-Meier curves for Arm 1: patients receiving Standard Combination Therapy (solid yellow line), Arm 2: Maintenance Treatment (solid cyan), Arm 3: Optimized dosing regimen determined through the *in silico* clinical trial (solid purple), Arm 4: GM-CSF monotherapy (dashed yellow line), and Arm 5: mono-virotherapy (dashed purple). Constrained optimization (Maintenance Therapy) outperforms standard combination therapy, despite additional limitations on dose timing.

tive strategy enabled us to analyze the effects of distinct therapy procedures on the *same* person, something which is clearly infeasible in the real world. Personalization of treatment regimens was achieved by simultaneously minimizing cumulative tumour and drug burdens. A probabilistic dosing regimen was subsequently defined based on the resulting personalized treatment schedules. Incorporating clinical realities, we determined that standard combination therapy was improved upon by both a maintenance strategy (where immunotherapy is administered evenly throughout each virotherapy cycle) and this probabilistic dosing strategy. The latter was shown to be significantly better than both monotherapy and standard-of-care combination approaches. It is worth noting that the maintenance type therapy is not significantly different than the optimized scheduling, illustrating the utility of model based optimization techniques in identifying and developing improved therapeutic strategies.

There are differences between the OPTiM trial and our *in silico* trial. First, while we can broadly recreate the number of individuals in each stage of disease, we cannot identically recreate the underlying distribution of patients. Accordingly, our results are highly depen-

dent on the virtual patients selected for participation based on their tumour doubling time, and would be improved through the incorporation of detailed staging and patient distribution data. Second, the administration of an oncolytic virus can lead to an anti-viral adaptive immune responses and a decrease in treatment efficacy that is currently not accounted for in the model. Last, our computational model simplifies tumour-immune interactions by lumping all immune cells into a single phagocyte population. We also considered a single cytokine as a cipher for all pro-inflammatory responses induced by tumour-immune communication. We believe that these considerations do not significantly impact on our general results, but they should be addressed in future work to increase the precision of the predicted personalized regimens. Additionally, the lack of empirically determined distributions for the model's parameter values limits our approach. Ideally, data for these measures would be available to strengthen the model's predictions. Nonetheless, our parameterization recapitulated the OPTiM trial results.

Despite these limitations, our results underline the contribution of computational biology to understanding the determinants of improved clinical care and support continued efforts towards rational therapy design. Significantly, this computational biology study suggests promising avenues of investigation towards tailored combination immunotherapy/oncolytic virotherapy for patients with late-stage melanoma.

Acknowledgements

Part of this work was performed while TC attended the *Mathematical Biology* thematic research program organized by the Mittag-Leffler Institute. TC and MC would like to thank Tony Humphries for discussions regarding this work.

Funding Information

TC was supported by Natural Sciences and Engineering Research Council of Canada (NSERC) PGS-D award. MC was supported by an NSERC Discovery Grant no. RGPIN-2018-04546.

Conflict of Interest

The authors declare no conflicts of interest.

Supplementary Information: Optimal Combination Immunotherapy/Oncolytic Virotherapy Determined Through *In Silico* Clinical Trials Improves Late Stage Melanoma Patient Outcomes

Tyler Cassidy, Morgan Craig

The computational biology model (described textually in Eq. (S1)) was based on the model of Cassidy and Humphries[28] and explicitly included heterogeneity in tumour cell reproduction velocity and tumour-immune interactions via a distributed delay differential equation. The model describes both quiescent and G_1 phase tumour cell populations while modelling the remainder of mitosis as a delayed process, and incorporates a phagocyte population and a proinflammatory cytokine that drives the tumour-immune interaction through increased phagocyte recruitment.

Let $Q(t)$ and $G_1(t)$ denote the quiescent and proliferative phase susceptible tumour cells, respectively, $C(t)$ denote the concentration of GM-CSF, $P(t)$ the phagocyte concentration in the tumour microenvironment, $V(t)$ the concentration of oncolytic virions, and $I(t)$ the number of infected tumour cells. Infection of susceptible tumour cells occurred at rate η, while tumour-immune interactions took place with rate $\psi_{Q,G}$.

To account for immune selection, we included a resistant strain of tumour cells undetectable to the immune system (represented by $Q_R(t)$, $G_{1,R}(t)$, analogous to the susceptible population). We assumed that tumour cells successfully completing mitosis could randomly mutate into the immune resistant strain with probability $\mu = 1 \times 10^{-10}$, and we assumed that the mutated strain of cancer cells reproduced identically to the non-mutated strain.

$$\left.\begin{aligned}
\tfrac{\mathrm{d}}{\mathrm{dt}}Q(t) &= \text{Mitotic Output} - \text{Transit to active phase} \\
&\quad -\text{Apoptosis} - \text{Immune Death} \\
\tfrac{\mathrm{d}}{\mathrm{dt}}G_1(t) &= \text{Transit from quiescence} - \text{Transit to Mitosis} \\
&\quad -\text{Apoptosis} - \text{Viral Infection} - \text{Immune Death} \\
\tfrac{\mathrm{d}}{\mathrm{dt}}I(t) &= \text{Viral infection} - \text{Death of infected cells} \\
\tfrac{\mathrm{d}}{\mathrm{dt}}V(t) &= \text{Dose}_V(t) + \text{Lysis} - \text{Viral infection} - \text{Virion death} \\
\tfrac{\mathrm{d}}{\mathrm{dt}}P(t) &= \text{Immune recruitment} - \text{Phagocyte death} \\
\tfrac{\mathrm{d}}{\mathrm{dt}}C(t) &= \text{Dose}_C(t) + \text{Cytokine Production} - \text{Renal clearance} \\
\tfrac{\mathrm{d}}{\mathrm{dt}}Q_R(t) &= \text{Development of Resistance} + \text{Mitotic Output} \\
&\quad -\text{Transit to active phase} - \text{Apoptosis} \\
\tfrac{\mathrm{d}}{\mathrm{dt}}G_{1,R}(t) &= \text{Transit from quiescence} - \text{Transit to Mitosis} \\
&\quad -\text{Apoptosis} - \text{Viral Infection.}
\end{aligned}\right\} \quad \text{(S1)}$$

The differential equations describing the progression of disease are

$$\left.\begin{aligned}
\tfrac{\mathrm{d}}{\mathrm{d}t}Q(t) &= 2(1-\mu)\int_{-\infty}^{t}\exp\left[-\int_{\sigma}^{t}\hat{d}_K+\eta(U(x))+\psi_G(U(x))\mathrm{d}x\right]a_2G_1(\sigma)K(t-\sigma)\mathrm{d}\sigma\\
&\quad -a_1Q(t)-d_1Q(t)-\psi_Q(U(t))Q(t)\\
\tfrac{\mathrm{d}}{\mathrm{d}t}G_1(t) &= a_1Q(t)-a_2G_1(t)-d_2G_1(t)-\eta(U(t))G_1(t)-\psi_G(U(t))G_1(t)\\
\tfrac{\mathrm{d}}{\mathrm{d}t}Q_R(t) &= 2\mu\int_{-\infty}^{t}\exp\left[-\int_{\sigma}^{t}\hat{d}_K+\eta(U(x))+\psi_G(U(x))\mathrm{d}x\right]a_2G_1(\sigma)K(t-\sigma)\mathrm{d}\sigma\\
&\quad -a_1Q_R(t)-d_1Q_R(t)\\
&\quad +2\int_{-\infty}^{t}\exp\left[-\int_{\sigma}^{t}\hat{d}_K+\eta(U(x))\mathrm{d}x\right]a_2G_{1,R}(\sigma)K(t-\sigma)\mathrm{d}\sigma\\
\tfrac{\mathrm{d}}{\mathrm{d}t}G_{1,R}(t) &= a_1Q_R(t)-a_2G_{1,R}(t)-d_2G_{1,R}(t)-\eta(U(t))G_{1,R}(t)\\
\tfrac{\mathrm{d}}{\mathrm{d}t}I(t) &= \eta(U(t))\left[G_1(t)+G_{1,R}(t)+N(t)\right]-\delta I(t)\\
\tfrac{\mathrm{d}}{\mathrm{d}t}V(t) &= \mathrm{Dose}_V(t)-\eta(U(t))\left[G_1(t)+G_{1,R}(t)+N(t)\right]+\alpha[\delta I(t)]-\omega V(t)\\
\tfrac{\mathrm{d}}{\mathrm{d}t}C(t) &= \mathrm{Dose}_C(t)+C_{prod}(U(t))-k_{elim}C(t)\\
\tfrac{\mathrm{d}}{\mathrm{d}t}P(t) &= \varphi(C(t))-\gamma_pP(t).
\end{aligned}\right\} \tag{S2}$$

The total number of cells in the cell cycle is given by

$$\begin{aligned}
N(t) = &\int_0^{\infty}a_2\exp\left[-\int_{t-\xi}^{t}\hat{d}_K+\eta(U(x))\mathrm{d}x\right]\left(1-\int_0^{\xi}K(\sigma)\mathrm{d}\sigma\right)\\
&\times\left(G_1(t-\xi)\exp\left[-\int_{t-\xi}^{t}\psi_G(U(x))\mathrm{d}x\right]+G_{1,R}(t-\xi)\right)\mathrm{d}\xi.
\end{aligned}$$

We modelled the subcutaneous administration of N doses of GM-CSF similar to Craig et al.[27] by

$$\mathrm{Dose}_C(t)=\sum_{i=1}^{N}\frac{k_a^cF_c\mathrm{Admin}_i^c(t)}{Vol}\exp\left[-k_a^c(t-t_i)\right], \tag{S3}$$

where the amount of GM-CSF administered at time t_i is Dose_i^c and

$$\mathrm{Admin}_i^c(t)=\begin{cases}0 & \text{if}\quad t<t_i\\ \mathrm{Dose}_i^c & \text{if}\quad t\geqslant t_i.\end{cases}$$

The parameter k_a^c denotes the absorption rate of GM-CSF, and F the bioavailable fraction of GM-CSF. Similarly, the intralesion administration of oncolytic viruses[11,12,40] was modelled as

$$\mathrm{Dose}_V(t)=\sum_{j=1}^{N}\frac{k_a^vF_v\mathrm{Admin}_i^v(t)}{Vol}\exp\left[-k_a^v(t-t_j)\right] \tag{S4}$$

where Dose_j^v is the amount of virus administered at time $t=t_j$ and

$$\mathrm{Admin}_j^v(t)=\begin{cases}0 & \text{if}\quad t<t_j\\ \mathrm{Dose}_j^v & \text{if}\quad t\geqslant t_j.\end{cases}$$

As we considered intralesional administration, $F_V = 1$. Further, absorption into the tumour was assumed to be much faster than cytokine absorption, so that $k_a^v >> k_a^c$. Equation (S2) was simulated using its finite dimensional representation.[28]

Simulation of the Mathematical Model

We simulated the model using the stiff ODE solver *ode15s* in Matlab[37] after reduction to a finite dimensional system of ODEs, obtained using the technique previously developed[28]

$$\left.\begin{aligned}
\tfrac{\mathrm{d}}{\mathrm{dt}}Q(t) &= 2(1-\mu)k_{tr}A_j(t) - a_1Q(t) - d_1Q - \psi_Q(U(t))Q(t)\\
\tfrac{\mathrm{d}}{\mathrm{dt}}G_1(t) &= a_1Q(t) - a_2G_1(t) - d_2G_1(t) - \psi_G(U(t))G_1(t) - \eta(U(t))G_1(t)\\
\tfrac{\mathrm{d}}{\mathrm{dt}}A_1(t) &= a_2G_1(t) - k_{tr}A_1(t)) - [\hat{d}_g + \eta(U(t)) + \psi_G(U(t))]A_1(t)\\
\tfrac{\mathrm{d}}{\mathrm{dt}}A_i(t) &= k_{tr}(A_{i-1}(t) - A_i(t)) - [\hat{d}_g + \eta(U(t)) + \psi_G(U(t))]A_i(t) \quad \text{for} \quad i = 2, 3..., j\\
\tfrac{\mathrm{d}}{\mathrm{dt}}Q_R(t) &= 2\mu k_{tr}A_j(t) + 2k_{tr}A_{j,R}(t) - a_1Q_R(t) - d_1Q_R(t)\\
\tfrac{\mathrm{d}}{\mathrm{dt}}G_{1,R}(t) &= a_1Q_R(t) - a_2G_{1,R}(t) - d_2G_{1,R}(t) - \eta(U(t))G_{1,R}(t)\\
\tfrac{\mathrm{d}}{\mathrm{dt}}A_{1,R}(t) &= a_2G_{1,R}(t) - k_{tr}A_{1,R}(t)) - [\hat{d}_g + \eta(U(t)) + \psi_G(U(t))]A_{1,R}(t)\\
\tfrac{\mathrm{d}}{\mathrm{dt}}A_{i,R}(t) &= k_{tr}(A_{i-1,R}(t) - A_{i,R}(t)) - [\hat{d}_g + \eta(U(t)) + \psi_G(U(t))]A_{i,R}(t) \quad \text{for} \quad i = 2, 3..., j\\
\tfrac{\mathrm{d}}{\mathrm{dt}}I(t) &= -\delta I(t) + \eta(U(t))\left[G_1(t) + N(t)\right]\\
\tfrac{\mathrm{d}}{\mathrm{dt}}V(t) &= \alpha\delta I(t) - \omega V(t) - \eta(U(t))\left[G_1(t) + N(t)\right]\\
\tfrac{\mathrm{d}}{\mathrm{dt}}C(t) &= C_{prod}(U(t)) - k_{elim}C(t)\\
\tfrac{\mathrm{d}}{\mathrm{dt}}P(t) &= \varphi(C(t)) - \gamma_pP(t)
\end{aligned}\right\} \tag{S5}$$

Parametrization of the Model

To begin, we converted tumour volumes to cell numbers by assuming that $1\,\mathrm{mm}^3 = 1 \times 10^6$ cells.[41] To accurately account for the heterogeneity in cell cycle time, we integrated the intermitotic time of cervical cancer cells measured by Sato et al.[42] There, the intermitotic time was determined by calculating the division time of a HeLa parent cell and then tracking the two daughter cells until their division. For each daughter cell, the intermitotic time was given by the time difference between birth and division, with a mean intermitotic time of 1.40 (standard deviation of $s = 0.28$ days). The intermitotic time measured by Sato et al. also includes the G_1 phase of the cell cycle. In (S2), cells that divide spend, on average, $1/a_2$ days in G_1. Thus, the mean of the delay kernel in (S2), τ, satisfies

$$\tau = 33.7/24 - 1/a_2, \tag{S6}$$

which provided a lower bound on the value of a_2. The gamma distribution has a density given by

$$g_b^j(t) = \frac{b^j}{\Gamma(j)} t^{j-1} \exp\left[-bt\right]$$

with mean $\tilde{x} = j/b$ and standard deviation $s^2 = \tau^2/j$. Thus, for a given value of a_2, we parametrized the delay kernel in (S2) by

$$j = \tau^2/s^2,$$

and

$$b = j/\tau.$$

To use the linear chain technique,[28] we enforced that $j \in \mathbb{N}$.

Dingli et al. administered myeloma cells to 6 week old irradiated and severely combined immunocomprimised mice and measured the increase in tumour volume over 40+ days. We digitized the data from their Figure 1 and used tumour growth in the absence of immune pressure to fit the tumour growth parameters a_1, a_2 and d_2. To reduce the number of parameters to be estimated, we fixed the apoptosis rate of quiescent cells to be $d_1 = 0$. Since the mice in the Dingli et al. study were immunocomprimised and no viral therapy was administered, we only considered the reduced system of $Q(t), S(t)$ and $N(t)$, and then calculated the distribution parameters using (S6) and $b = j/\tau$. As only the initial number of tumour cells (and not their distribution across the cell cycle) is known for each mouse, we distributed the initial inncoulum of tumour cells across quiescent and the active portions of the cell cycle according to the proportion of time spent in each phase. Then, for each parameter set, we simulated the reduced mathematical model and minimized the least-squares error between model predictions and the data from Figures 1 (a) and (c) in Dingli et al. using the *fmincon* function in Matlab (Fig. S1). **I know it's trivial but let's have one equation of the error calculation.**

Viral and infected cell kinetic parameters were determined using *in vitro* and *in vivo* studies of T-VEC kinetics and data from Toda et al.[43] In their study, Toda et al. injected murine melanoma cells into mice and waited for the tumours reached 5 mm in size. At that point, defective HSV virus encoding for GM-CSF was injected into the tumour. The increase in tumour volume as compared with untreated control mice was measured over 15 days. To fit this data, we fixed the tumour growth parameters a_1, a_2, d_1 and d_2 from the Dingli et al. estimates and simulated tumour growth during 15 days. Then, for a fixed parameter set $[\kappa, \eta_{1/2}, \omega, \delta, \alpha]$, we simulated the administration of one dose of oncolytic virus (supplied in 1 mL vials with a concentration of 1×10^6 PFU/mL or 1×10^8 PFU/mL). We then normalized the treated simulation against the control simulation.

To reduce identifiability issues, we also integrated data from Randazzo et al.[44] There, an oncolytic HSV virus was mixed with tumour cells *in vitro* and the proportion of viable cells was studied for different multiplicities of infection. As before, we fixed the tumour growth parameters and, for a given parameter set $[\kappa, \eta_{1/2}, \omega, \delta, \alpha]$, simulated infection and calculated the percentage of viable (non-infected) cells. For each of the Toda et al. and Randazzo et al. datasets, we calculated the least-squares error between simulations and data and minimized the sums of their errors (Fig. S2).

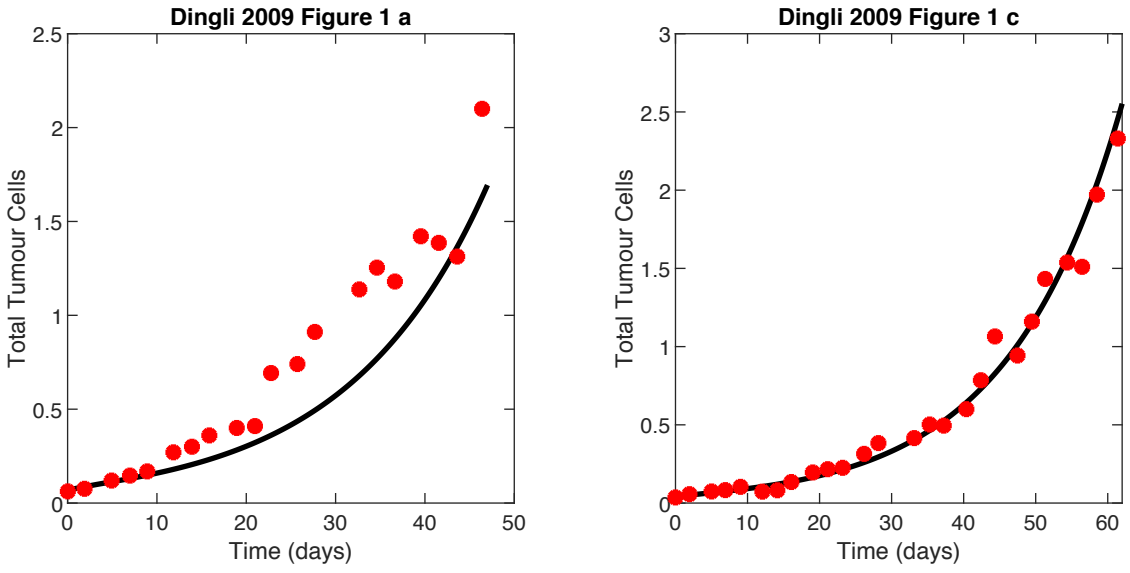

(a) (b)

Figure S1: **The results of the fitting algorithm for the tumour growth parameters.** Data (red circles) from Dingli et al.[41] for tumour growth in immunocompromised mice compared to model predictions (solid black lines).

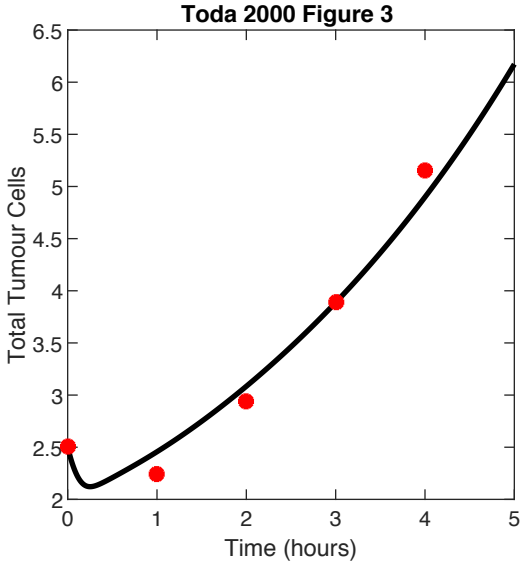

Figure S2: **The results of the parameter fitting algorithm for the viral parameters.** Comparisons of model predictions (solid black lines) and the Toda et al. data[43] (red circles) for the number of viable cells following the administration of T-VEC.

Due to the lack of PopPK/semi-mechanistic models of GM-CSF, we adapted a model[27] for granulocyte colony stimulating factor (G-CSF), a similar protein, that includes both neutrophil mediated and renal clearance of circulating G-CSF. Since we were primarily interested in immune cells that do not have a G-CSF receptor (macrophages and T-cells), we did not consider neutrophil mediated clearance and fixed $k_{elim} = 0.16139$ 1/day. The basal concentration of GM-CSF in healthy patients is 2.43 pg/mL,[45] given by

$$C^* = \frac{C^*_{prod}}{k_{elim}},$$

at homeostasis. Thus,

$$C^*_{prod} = k_{elim} C^* = 0.00039863 \text{ng/mL/day}.$$

To calculate the maximal cytokine production, C^{max}_{prod}, we considered experimental data from Liu et al.[46] from the injection of carcinoma cells into mice. Therein, different MOIs of oncolytic HSV virus expressing GM-CSF was administered after a period of initial tumour growth. Throughout, circulating GM-CSF was measured through ELISA. To replicate the experimental set up, we simulated the administration of oncolytic virus in and minimized the least-squares error between the simulation and the experimental data for fixed parameter values $[C^{max}_{prod}, C_{1/2}]$, while holding the tumour growth and viral dynamics at their previously estimated values.

The parametrization of the immune compartment was based on Barish et al.,[47] where a mathematical model of murine tumour growth in the presence of a competent immune system and dendritic cell vaccine was developed. The structure of the Barish et al. model of immune dynamics is quite similar to our differential equation for $P(t)$. There, the rate of conversion from dendritic cell activation to recruitment of active anti tumour T-cells was given by $\chi_X = 4.6754$, which we adopted directly ($k_{cp} = \chi_X = 4.6754$). We also set the clearance rate of phagocytes to be the same as the clearance rate of T-cells, so $\gamma_p = \delta_T = 0.35$. The remaining immune involvement parameters, k_p and $k_q = k_s$, were set to ensure that the average patient had a tumour doubling time that fell near the center of the range found in patients with late stage melanoma.[29] Parameters values for an average patient (see main section *Generation of In Silico Individuals and Patient Cohorts*) are provided in Table S1.

Virtual Population Patient Distribution and History Function Derivation

The distribution of disease stage in the OPTiM trial was a crucial component for considering the overall survival statistics given the decreased 5 year survival rate for patients with more advanced disease. The original trial registered patients with not surgically resectable stage IIIB to IV melanoma. In the T-VEC cohort, 30% of patients had stage 3 melanoma. The median progression time from first treatment to lymph metastases was 18 months, while the median time to distant metastases was 24 months.[48] To reproduce this distribution of disease stage in our virtual population, for each of the 30% of virtual patients with stage

Parameter	Value	Biological Interpretation (Unit)
a_1	1.183	Quiescent to interphase rate (1/day)
d_1	0	Quiescent death rate (1/day)
a_2	1.758	Interphase to active phase rate (1/day)
d_2	0.539	Interphase death rate (1/day)
d_3	0.539	Active phase death rate (1/day)
$\hat{d}_g$	0.167	Active phase death rate (1/day)
κ	3.53	Virion contact rate (1/day)
$\eta_{1/2}$	0.51	Virion half effect concentration (virions)
δ	4.96	Lysis rate (1/day)
α	0.00829	Lytic virion release rate (virions/cell)
ω	9.686	Virion death rate (1/day)
k_{cp}	4.675	Maximal phagocyte production rate (10^{10} cells/day)
$C_{1/2}$	0.739	Phagocyte production half effect (ng/mL/day)
$\Psi_{1/2}$	5	Cytokine production half effect (10^{10} cells/day)
γ_p	0.35	Phagocyte death rate (1/day)
C^*_{prod}	3.98×10^{-4}	Homeostatic cytokine production rate (ng/mL/day)
C^{max}_{prod}	1.429	Maximal cytokine production rate (ng/mL/day)
k_{elim}	0.16139	Cytokine elimination rate (1/day)
k_p	0.05	Phagocyte-tumour cell contact rate (1/day)
$k_{q,s}$	10	Phagocyte cell digestion constant
τ	0.8354	Expected cell cycle duration (day)

Table S1: The vector $\mathbf{p}$ (see main section *Generation of in-silico individuals and patient cohorts*) with biological interpretations. See Cassidy and Humphries[28] for detailed descriptions of each parameter.

3 melanoma, we assumed that initial treatment was discontinued sometime s_0 in the past, where s_0 was sampled uniformly from $[16, 20]$. Similarly, for the 70% of virtual patients with stage 4 melanoma, we sampled s_0 uniformly from $[22, 26]$.

To set the history function φ_G for (S2), we assumed that there was a tumour of size $T_0 > 0$ at cessation of the initial therapy. We began by modelling untreated tumour growth by

$$\frac{\mathrm{d}}{\mathrm{dt}}\left[Q(s) + G_1(s)\right] \approx \frac{\mathrm{d}}{\mathrm{dt}}T(s) = \left[2a_2 \exp[-d_3\tau] - a_2 - d_2\right] T(s), \quad s \in [s_0, 0].$$

Thus, at the beginning of treatment, the total number of tumour cells for each patient was

$$T_0 \exp\left[\left(2a_2 \exp[-d_3\tau] - a_2 - d_2\right) s_0\right].$$

We distributed these tumour cells across the quiescent, G_1, and mitotic populations according to the expected fraction of time spent in each population. In practice, however, it is simpler to implement the varied initial conditions by adjusting the tumour size at removal.

Local Sensitivity Analysis and Population Composition

Potential drug targets were identified by performing a sensitivity analysis on the mathematical model's parameters. Each parameter was varied one-by-one by 10%. The influence of each of these variations was measured by comparing the predicted tumour doubling time and the tumour burden after 15 months to the model's predictions without any parameter changes according to

$$\%\text{ change in tumour burden} = 100\% \times \frac{\text{Tumour burden with parameter change}}{\text{Tumour burden without parameter change}}.$$

The parameters controlling the dynamics of mitotic cells were the most sensitive, with the 10% change accounting for drastic changes in disease burden. For example, increasing the rate at which G_1 cells enter into mitosis results in a 11-fold increase in tumour burden, while decreasing this rate decreased the tumour burden by a factor of 33 (Figure S3), indicating that interventions that inhibit the specific transition from G_1 into mitosis offer consequential therapeutic benefits.

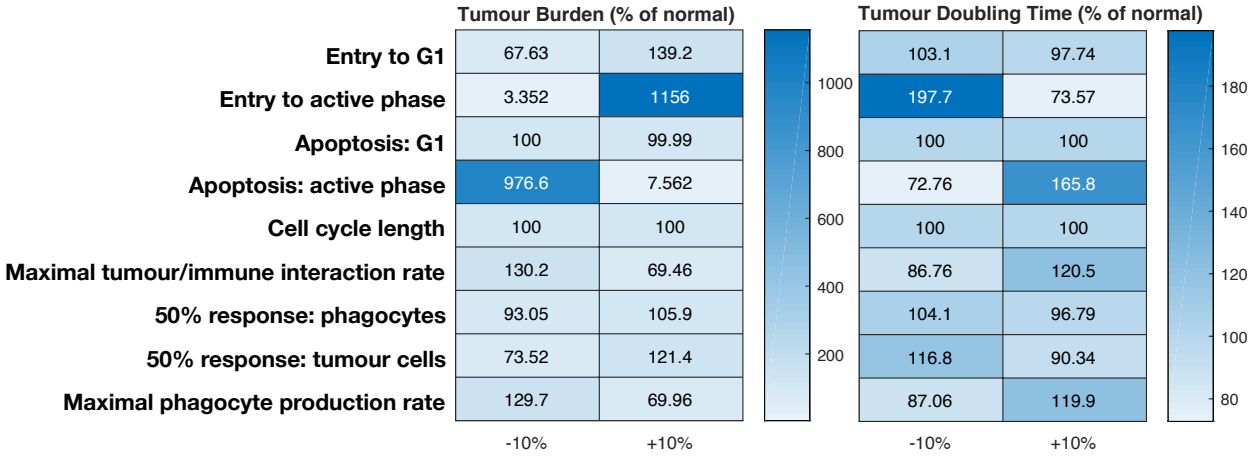

Figure S3: **Heat map of local parameter sensitivity analysis.** Figure (a) shows the dependence of tumour burden on the parameters shown on the y-axis. Figure (b) shows the dependence of tumour doubling time on the parameters shown on the y-axis. In both cases, parameters were varied by ±10%.

References

[1] D. Basanta, J. G. Scott, M. N. Fishman, G. Ayala, S. W. Hayward, and A. R. A. Anderson, "Investigating prostate cancer tumourÔÇôstroma interactions: clinical and biological insights from an evolutionary game," *Br. J. Cancer*, vol. 106, pp. 174–181, jan 2012.

[2] R. Venkatasubramanian, R. B. Arenas, M. A. Henson, and N. S. Forbes, "Mechanistic modelling of dynamic MRI data predicts that tumour heterogeneity decreases therapeutic response," *Br. J. Cancer*, vol. 103, pp. 486–497, aug 2010.

[3] S. J. Russell, K.-W. Peng, and J. C. Bell, "Oncolytic virotherapy," *Nat. Biotechnol.*, vol. 30, pp. 658–670, jul 2012.

[4] I. Mellman, G. Coukos, and G. Dranoff, "Cancer immunotherapy comes of age," *Nature*, vol. 480, pp. 480–489, dec 2011.

[5] H. Fukuhara, Y. Ino, and T. Todo, "Oncolytic virus therapy: A new era of cancer treatment at dawn," *Cancer Sci.*, vol. 107, no. 10, pp. 1373–1379, 2016.

[6] H. A. Hoster, R. P. Zanes, and E. von Hamm, "The Association of "Viral" Hepatitis and Hodgkin's Disease," *Cancer Res.*, vol. 9, no. 8, pp. 473–480, 1949.

[7] E. A. Chiocca and S. D. Rabkin, "Oncolytic viruses and their application to cancer immunotherapy," *Cancer Immunol. Res.*, vol. 2, no. 4, pp. 295–300, 2015.

[8] K. Cassady, K. Haworth, J. Jackson, J. Markert, and T. Cripe, "To infection and beyond: The multi-pronged anti-cancer mechanisms of oncolytic viruses," *Viruses*, vol. 8, p. 43, feb 2016.

[9] C. J. Breitbach, B. D. Lichty, and J. C. Bell, "Oncolytic viruses: Therapeutics with an identity crisis," *EBioMedicine*, vol. 9, pp. 31–36, 2016.

[10] G. Marelli, A. Howells, N. R. Lemoine, and Y. Wang, "Oncolytic Viral Therapy and the Immune System: A Double-Edged Sword Against Cancer," *Front. Immunol.*, vol. 9, pp. 1–8, apr 2018.

[11] R. H. I. Andtbacka, H. L. Kaufman, F. Collichio, T. Amatruda, N. Senzer, J. Chesney, K. A. Delman, L. E. Spitler, I. Puzanov, S. S. Agarwala, M. Milhem, L. Cranmer, B. Curti, K. Lewis, M. Ross, T. Guthrie, G. P. Linette, G. A. Daniels, K. Harrington, M. R. Middleton, W. H. Miller, J. S. Zager, Y. Ye, B. Yao, A. Li, S. Doleman, A. Van Der Walde, J. Gansert, and R. S. Coffin, "Talimogene laherparepvec improves durable response rate in patients with advanced melanoma," *J. Clin. Oncol.*, vol. 33, no. 25, pp. 2780–2788, 2015.

[12] P. K. Bommareddy, A. Patel, S. Hossain, and H. L. Kaufman, "Talimogene Laherparepvec (T-VEC) and Other Oncolytic Viruses for the Treatment of Melanoma," *Am. J. Clin. Dermatol.*, vol. 18, no. 1, pp. 1–15, 2017.

[13] H. Rehman, A. W. Silk, M. P. Kane, and H. L. Kaufman, "Into the clinic: Talimogene laherparepvec (T-VEC), a first-in-class intratumoral oncolytic viral therapy," *J. Immunother. Cancer*, vol. 4, no. 1, pp. 1–8, 2016.

[14] A. Mostafa, D. Meyers, C. Thirukkumaran, P. Liu, K. Gratton, J. Spurrell, Q. Shi, S. Thakur, and D. Morris, "Oncolytic Reovirus and Immune Checkpoint Inhibition as a Novel Immunotherapeutic Strategy for Breast Cancer," *Cancers (Basel).*, vol. 10, p. 205, jun 2018.

[15] J. Chesney, I. Puzanov, F. Collichio, P. Singh, M. M. Milhem, J. Glaspy, O. Hamid, M. Ross, P. Friedlander, C. Garbe, T. F. Logan, A. Hauschild, C. Lebbé, L. Chen, J. J. Kim, J. Gansert, R. H. Andtbacka, and H. L. Kaufman, "Randomized, Open-Label Phase II Study Evaluating the Efficacy and Safety of Talimogene Laherparepvec in Combination With Ipilimumab Versus Ipilimumab Alone in Patients With Advanced, Unresectable Melanoma," *J. Clin. Oncol.*, vol. 36, pp. 1658–1667, jun 2018.

[16] Z. S. Guo and D. L. Bartlett, "Oncolytic viruses as platform for multimodal cancer therapeutics: a promising land," *Cancer Gene Ther.*, vol. 21, pp. 261–263, jul 2014.

[17] S. E. Lawler and E. A. Chiocca, "Oncolytic virus-mediated immunotherapy: A combinatorial approach for cancer treatment," *J. Clin. Oncol.*, vol. 33, no. 25, pp. 2812–2814, 2015.

[18] J. Bell and G. McFadden, "Viruses for tumor therapy," *Cell Host Microbe*, vol. 15, no. 3, pp. 260–265, 2014.

[19] S. Chaurasiya, N. G. Chen, and Y. Fong, "Oncolytic viruses and immunity," *Curr. Opin. Immunol.*, vol. 51, pp. 83–90, apr 2018.

[20] N. T. Martin and J. C. Bell, "Oncolytic Virus Combination Therapy: Killing One Bird with Two Stones," *Mol. Ther.*, vol. 26, no. 6, pp. 1414–1422, 2018.

[21] R. J. Allen, T. R. Rieger, and C. J. Musante, "Efficient Generation and Selection of Virtual Populations in Quantitative Systems Pharmacology Models," *CPT Pharmacometrics Syst. Pharmacol.*, vol. 5, pp. 140–146, mar 2016.

[22] Z. Agur, "From the evolution of toxin resistance to virtual clinical trials: the role of mathematical models in oncology," *Futur. Oncol.*, vol. 6, no. 6, pp. 917–927, 2010.

[23] B. J. Schmidt, F. P. Casey, T. Paterson, and J. R. Chan, "Alternate virtual populations elucidate the type I interferon signature predictive of the response to rituximab in rheumatoid arthritis," *BMC Bioinformatics*, vol. 14, no. 1, p. 221, 2013.

[24] S. B. Love, S. Brown, C. J. Weir, C. Harbron, C. Yap, B. Gaschler-Markefski, J. Matcham, L. Caffrey, C. McKevitt, S. Clive, C. Craddock, J. Spicer, and V. Cornelius, "Embracing model-based designs for dose-finding trials," *Br. J. Cancer*, vol. 117, pp. 332–339, jul 2017.

[25] J. Zhang, J. J. Cunningham, J. S. Brown, and R. A. Gatenby, "Integrating evolutionary dynamics into treatment of metastatic castrate-resistant prostate cancer," *Nat. Commun.*, vol. 8, p. 1816, dec 2017.

[26] M. Bentele, I. Lavrik, M. Ulrich, S. Stößer, D.W. Heermann, H. Kalthoff, P.H. Krammer, and R. Eils, "Mathematical modeling reveals threshold mechanism in CD95-induced apoptosis," *J. Cell Biol.*, vol. 166, pp. 839–851, 2014.

[27] M. Craig, A.R. Humphries, M.C. Mackey, "A mathematical model of granulopoiesis incorporating the negative feedback dynamics and kinetics of G-CSF/neutrophil binding and internalization," *Bull. Math. Biol.*, vol. 78(12), pp. 2304-2357, 2016.

[28] T. Cassidy and A. R. Humphries, "A mathematical model of viral oncology as an immuno-oncology instigator," *Math. Med. Biol. A J. IMA*, vol. To appear, 2019.

[29] J. A. Carlson, "Tumor doubling time of cutaneous melanoma and its metastasis," *Am. J. Dermatopathol.*, vol. 25, pp. 291–299, aug 2003.

[30] P. Klasse, "Molecular Determinants of the Ratio of Inert to Infectious Virus Particles," vol. 118, pp. 285–326, 2015.

[31] R. Stadler, T. Luger, T. Bieber, U. Köhler, R. Linse, K. Technau, R. Schubert, K. Schroth, F. Vakilzadeh, M. Volkenandt, H. Gollnick, H. Von Eick, F. Thoren, and Ö. Strannegård, "Long-term survival benefit after adjuvant treatment of cutaneous melanoma with dacarbazine and low dose natural interferon alpha: A controlled, randomised multicentre trial," *Acta Oncol. (Madr).*, vol. 45, pp. 389–399, jan 2006.

[32] V. P. Collins, R. K. Loeffler, and H. Tivey, "Observations on growth rates of human tumors," *Amer. J. Roentgenol.*, vol. 76, pp. 988–1000, 1956.

[33] M. Schwartz, "A biomathematical approach to clinical tumor growth," *Cancer*, vol. 14, pp. 1272–1294, nov 1961.

[34] J. Holland, "Genetic Algorithms," *Sci. Am.*, no. July, 1992.

[35] J. Holland, *Adaptation in natural and artificial systems: An introductory analysis with applications to biology, control, and artificial intelligence*. Cambridge, Massachusetts: The MIT Press, 1 ed., 1975.

[36] J. McCall, "Genetic algorithms for modelling and optimisation," *J. Comput. Appl. Math.*, vol. 184, pp. 205–222, dec 2005.

[37] MATLAB, *R2017a*. Natick, Massachusetts: The MathWorks Inc., 2017.

[38] A. Aitken, D. Roy, and M.-C. Bourgeois-Daigneault, "Taking a Stab at Cancer; Oncolytic Virus-Mediated Anti-Cancer Vaccination Strategies," *Biomedicines*, vol. 5, p. 3, jan 2017.

[39] G. P. Dunn, A. T. Bruce, H. Ikeda, L. J. Old, and R. D. Schreiber, "Cancer immunoediting: From immunosurveillance to tumor escape," *Nat. Immunol.*, vol. 3, no. 11, pp. 991–998, 2002.

[40] D. B. Johnson, I. Puzanov, and M. C. Kelley, "Talimogene laherparepvec (T-VEC) for the treatment of advanced melanoma," *Immunotherapy*, vol. 7, pp. 611–619, jul 2015.

[41] D. Dingli, C. Offord, R. Myers, K. W. Peng, T. W. Carr, K. Josic, S. J. Russell, and Z. Bajzer, "Dynamics of multiple myeloma tumor therapy with a recombinant measles virus," *Cancer Gene Ther.*, vol. 16, no. 12, pp. 873–882, 2009.

[42] S. Sato, A. Rancourt, Y. Sato, and M. S. Satoh, "Single-cell lineage tracking analysis reveals that an established cell line comprises putative cancer stem cells and their heterogeneous progeny," *Sci. Rep.*, vol. 6, p. 23328, sep 2016.

[43] M. Toda, R. L. Martuza, and S. D. Rabkin, "Tumor Growth Inhibition by Intratumoral Inoculation of Defective Herpes Simplex Virus Vectors Expressing GranulocyteÔÇô-Macrophage Colony-Stimulating Factor," *Mol. Ther.*, vol. 2, pp. 324–329, oct 2000.

[44] B. P. Randazzo, M. G. Bhat, S. Kesari, N. W. Fraser, and S. M. Brown, "Treatment of experimental subcutaneous human melanoma with a replication-restricted herpes simplex virus mutant," *J. Invest. Dermatol.*, vol. 108, no. 6, pp. 933–937, 1997.

[45] J. Lee, Y. Kim, J. Lim, M. Kim, and K. Han, "G-CSF and GM-CSF concentrations and receptor expression in peripheral blood leukemic cells from patients with chronic myelogenous leukemia," *Ann. Clin. Lab. Sci.*, vol. 38, no. 4, pp. 331–337, 2008.

[46] H. Liu, "Preclinical evaluation of herpes simplex virus armed with granulocyte-macrophage colony-stimulating factor in pancreatic carcinoma," *World J. Gastroenterol.*, vol. 19, no. 31, p. 5138, 2013.

[47] S. Barish, M. F. Ochs, E. D. Sontag, and J. L. Gevertz, "Evaluating optimal therapy robustness by virtual expansion of a sample population, with a case study in cancer immunotherapy," *Proc. Natl. Acad. Sci.*, vol. 114, pp. E6277–E6286, aug 2017.

[48] F. Meier, S. Will, U. Ellwanger, B. Schlagenhauff, B. Schittek, G. Rassner, and C. Garbe, "Metastatic pathways and time courses in the orderly progression of cutaneous melanoma," *Br. J. Dermatol.*, vol. 147, no. 1, pp. 62–70, 2002.